AIAA-95-1828
Aerodynamic Characteristics of a Vertical Takeoff Vertical Landing (VTVL) Single Stage to Orbit Vehicle from M_∞= 0.1 to 10

W. C. Woods and N. R. Merski
NASA Langley Research Center
Hampton, VA

13th Applied Aerodynamics Conference
June 19 - 22 / San Diego, CA

AERODYNAMIC CHARACTERISTICS OF A VERTICAL TAKEOFF VERTICAL LANDING SINGLE STAGE TO ORBIT VEHICLE FROM M_∞ = 0.1 TO 10

W. C. Woods* and N. R. Merski**
NASA Langley Research Center
Hampton, VA 23681-0001

Abstract

Future access to space studies have considered a wide variety of follow on options to augment/replace the Space Shuttle. One option is a vertical takeoff and landing single stage to orbit vehicle. Experimental aerodynamic characteristics have been obtained on a generic design representative of such a vehicle; i.e., spherical nose blunting, a forebody of revolution and flat surfaces on the afterbody to accommadate control surfaces. Data has been obtained at subsonic, supersonic, and hypersonic Mach numbers to aid in determining cross range capability and performance, stability and control characteristics. The baseline configuration is longitudinally and laterally unstable, but appears to have the control authority to provide trim and stability augmentation. At subsonic speeds and angles of attack above 30° large lateral forces occur at zero sideslip and the lateral/directional characteristics are not well behaved.

Nomenclature

b	span, 3.756 inches
$\bar{c}$	mean aerodynamic chord, 3.756 inches
C_A	axial-force coefficient
C_D	drag coefficient
C_L	lift coefficient
$C_{L,\alpha}$	$\Delta C_L/\Delta\alpha$, per degree
C_l	rolling moment coefficient
C_m	pitching moment coefficient
C_N	normal force coefficients
C_n	yawing moment coefficient
$C_{n,\beta}$	$\Delta C_n/\Delta\beta$, per degree
C_Y	side-force coefficient
h	height, inches
L	length, inches
M	Mach number
R	unit Reynolds number, $\rho\frac{V}{\mu}$, per ft
r	radius, inches
S	reference area, square inches
$x_{c.g.}$	center of gravity location (moment reference center), 0.7 L_V
V	velocity, ft/sec^2
α	angle of attack, degrees
β	angle of sideslip, degrees
δ	control surface deflection (positive away from the body), degrees
ρ	density, slugs/ft^3
μ	viscosity, lb.-sec/ft^2

Subscripts

b	bottom, base
r	right
v	virtual origin
∞	free stream conditions

Introduction

NASA's initial manned space flight programs depended upon all expendable, series staged vehicles (Mercury, Gemini, Apollo, etc.) The requirement for routine access to low earth orbit coupled to the expense of flying expendable systems only once stimulated NASA to seek a cheaper, all reusable alternative.

---

* Research Engineer, Aerothermodynamics Branch, Gas Dynamics Division, Associate Fellow AIAA.
** Research Engineer, Aerothermodynamics Branch, Gas Dynamics Division, Member AIAA.

This became the genesis of the shuttle program in the late 1960's with a goal of hardware reusability and reducing the price of placing payload in orbit to under $100/lb in 1970 dollars. The shuttle program produced an outstanding system that accomplished many firsts: a man rated parallel staging system using solid rocket boosters; reusable throttleable rocket engines; and a reusable winged orbiter that glides to a runway landing. However, complete reusability was not obtained and the original cost reduction goal not achieved. While the shuttle is an amazing technological achievement, particularly when all the individual accomplishments necessary to make the system work are considered, it is deemed quite expensive to operate.

Single stage to orbit (SSTO) alternatives to shuttle were being considered before the first shuttle flight (Ref. 1). This approach to complete reusability and hopefully reduced cost has been the subject of numerous studies over the last two decades (e.g. Refs. 1 thru 3). In 1991, the Strategic Defense Initiative Office (SDIO) initiated studies to develop SSTO hardware that resulted in the development of a vertical takeoff, vertical landing (VTVL) concept by McDonnell Douglas Aerospace Co. (MDAC) called the Delta Clipper (Ref. 4). A 1/3 scale vehicle, called the DC-X, has been flown several times demonstrating system reusability, ground handling, and turn around time between flights, in addition to ascent, hover, translation and descent to safe touchdown capability.

One operational scenario for VTVL vehicles includes: a vertical liftoff and acceleration into orbit; a conventional nose forward entry at some moderate angle of attack; and an unconventional subsonic turn around maneuver to a base first vertical descent to landing (Fig. 1). The DC-X systems have demonstrated outstanding control in the terminal descent area. Entry aerodynamics and the subsonic turn around maneuver are yet to be demonstrated. MDAC conducted subsonic ground based tests, both power off and power on supporting the DC-X flight test program. However, an aerodynamic data base via wind tunnel testing across the speed range has not been established.

The Langley Research Center's Aerothermodynamics Branch performs aerothermodynamic research supporting the development of space transportation systems. An integral part of this program is the development of an experimental data base to identify possible problem areas VTVL vehicles may encounter across the speed range and to produce data to support 6-degree of freedom simulation of required maneuvers. This paper presents summary results of a preliminary experimental investigation to determine the stability and control characteristics of a generic vertical takeoff and landing vehicle from M_∞ = 0.1 to M_∞ = 10 at Reynolds numbers on the order of 2 x 10^6 per ft.

Apparatus and Tests

The baseline configuration for this study is a spherically blunted 8° half angle cone forebody that intersects with a cylindrical section at 88.4% of the length from the virtual origin. Planes, 90° apart parallel to the body's centerline, cut through the cylinder and the rear portion of the cone producing flat areas for locating 4 control flaps around the body for both longitudinal and lateral control. Each can be deflected from 0° to 40° in 10° increments and has an area 0.27S. Two blunt nose are considered (r_n/h_b = 0.1, 0.3). Figure 2(a) presents the geometric details of the body. Four fin like structures are located on the 45° diagonals. These structures were added to be aeroshell shrouds (or fairings) over the landing gears located in the base. Planform area for each fin is 0.07S. Figure 2(b) is a drawing of the configuration showing the relative location of control flaps and fins (landing gear covers). Figure 3 is a photograph of the model showing both noses and deflected flaps. The stagnation regions (noses), flaps, and fins were machined from stainless steel to be thermally compatible with the high stagnation temperatures of hypersonic facilities. The major part of the body was machined from aluminum to reduce model weight and cost (differences in machining time between stainless and aluminum). The model size was selected so that the more blunt nose configuration was 12" in length, resulting in the length for the less blunt nose configuration being approximately 14 inches. This size allowed one model to be tested across the speed range (M_∞ = 0.1 and M_∞ = 1.6 to 10) for a range of angle of attack of -5° to 70° and side slip of ±5°.

A wide variety of wind tunnels were used to produce the present data base (see Table 1). The ViGYAN Associates 3 ft x 4 ft Tunnel and the LaRC Low Turbulence Pressure Tunnel produced the subsonic results. The LaRC Unitary Plan Wind Tunnel Complex (test sections 1 and 2) was used from M_∞ = 1.6 to 4.5 and the Langley 20-inch Mach 6 and 31-inch Mach 10 Tunnels the M = 6 and 10 data. Additional information on these facilities can be found in Refs. 6-8. Test conditions are listed in Table 1. Model installation in the Unitary Plan Wind Tunnel is shown in fig. 4.

Aerodynamic forces and moments were measured using a sting-mounted 6 component strain gage balance. Base and/or model cavity pressures were measured using electronically scanned pressure systems. For all but subsonic conditions, base pressure effects were

subtracted from measured axial force. Moments are referenced to a moment center located at 70% of the length from the virtual origin. The circular diameter of the cylindrical afterbody (3.756 in)(not the distance across the flats) is used for both the chord and span and the reference area is the circular area based on that diameter (11.081 in^2). At subsonic conditions (the lowest dynamic pressure) accuracy of C_N, C_m, and the other components are ±0.12, ±0.03, and ± 0.0068 respectively. These are a worst case. Generally symbol size reflects data accuracy.

Techniques to fix transition were not used at subsonic and hypersonic conditions. The techniques recommended in ref. 9 were applied at M_∞ = 1.6 to 4.5.

Discussion of Results

Even as configuration aerolines were evolving, testing was initiated in various facilities to assess aerodynamic characteristics; thus the process was quite interactive. Because of the fast paced nature of this process, there are omissions at various Mach numbers. The baseline geometry with both noses and all flaps was fabricated initially and tested at M_∞ = 0.15 in the ViGYAN facility, at M_∞ = 2.5 - 4.5 in UPWT test section 2 and at M_∞ = 10 in the 31-Inch Mach 10 Tunnel. After the landing gear covers were fabricated their influence was determined at M_∞ = 0.1 to 0.25 in the Low Turbulence Pressure Tunnel, at M = 1.6 to 4. 5 in both UPWT test sections and at M_∞ = 6 in the 20-inch Mach 6 Tunnel.

Considering the large matrix of geometric parameters, two noses, fins off and on, and various flap combiniations, a large data base was produced. A discussion of the complete data base is beyond the scope of this paper. For this discussion basic aerodynamics will be presented across the Mach number range with specific results being presented at subsonic and hypersonic speeds.

Mach Number Effects

The effects of Mach number, nose bluntness and fins on initial lift curve slope ($C_{L,\alpha}$), minimum drag ($C_{D,o}$), and initial pitching moment curve slope ($C_{m,\alpha}$) are presented in figure 5. The general trend with increasing Mach number is a reduction of lift and drag as could be expected. The effect of Mach number on pitch is strongly dependent on nose bluntness with an increase in $C_{m,\alpha}$ (destabilizing) with increasing M_∞ occurring for r_n/h_b = 0.1 and a decrease in $C_{m,\alpha}$ (stabilizing) with increasing M_∞ occurring for r_n/h_b = 0.3. Increasing nose bluntness reduced $C_{L,\alpha}$ and increased $C_{D,o}$ at all Mach numbers. Adding the fins increased $C_{L,\alpha}$ and $C_{D,o}$and reduced $C_{m,\alpha}$ (stabilizing influence) at all Mach numbers. In general, the aerodynamic stability and control behavior from M_∞ = 1.6 to 6 followed expected trends.

Subsonic Aerodynamics

To provide preliminary information on the aerodynamic characteristics leading up to the subsonic turn around maneuver, high α data is essential. The ViGYAN facility has an α range from -10° to 70° for a straight sting and was used for initial subsonic testing. Figure 6 illustrates subsonic body axis data for the VTVL vehicle at M_∞ = 0.15 and R_∞ = 1.15 x 10^6/ft obtained in the ViGYAN tunnel. The vehicle had the 0.3 r_n/h_b nose installed with no fins and the controls set at zero. There is an increase in normal force curve slope at α>25°. This appears characteristic of the onset of vortex lift. The lateral directional data at β = 0° [fig. 6(b)] shows large side force (C_Y) occurring at α >25° . Apparently with the onset of vortex lift, unsymetrical crossflow separation and vortex sheading and reattachment is producing not only out of plane side force and yawing moment but also rolling moments. This is not an a surprising phenomena. Both fighters and missiles experience these forces when maneuvering at high speeds, and research in this area has been proceeding for a number of years (ref. 10, 11). The DC-X vehicle has fences at 45° intervals around its nose as a possible control of these effects. Because these fences could cause hypersonic heating problems, they were excluded for the present generic configuration.

Figure 7 illustrates the effect of Reynolds number at subsonic conditions. Results from ViGYAN and LTPT for the 0.3 r_n/h_b nose, zero controls, and fins off are presented. A dogleg sting/strut had to be applied in the LTPT to obtain data at angles of attack above 40° resulting in the lowest available α being 10°. Exact M_∞, R_∞ matches between the two facilities were not tested, but the trend with Reynolds number is well defined. General agreement in C_N between the two facilities exist as α is increased to 20° , where upon the previously shown ViGYAN results at R_∞ = 1.15 x 10^6/ft developed a marked increase in slope ($C_{N,\alpha}$)[fig. 7(a)]. LTPT results at R_∞ = 1.66 x 10^6/ft showed this departure in C_N to occur at α = 25° and for R_∞ = 3 x 10^6/ft the departure doesn't appear for the range of α tested. A strong influence of Reynolds number on side force coefficient is shown in fig. 7(b). Side force at β = 0° is shown to depart from zero at α = 30° at all Reynolds numbers with the largest side force occurring in ViGYAN at R_∞ = 1.15 x 10^6/ft; that is, the lowest value of Reynolds number. The LTPT test at R_∞ = 1.66 x

10^6/ft produced reduced side force, but had to be terminated at $\alpha = 30°$ due to unsteady forces on the model becoming too large and violent. Results at $R_\infty = 3 \times 10^6$ show reduced side force magnitude and opposite direction, with the side force coefficient being reduced an order of magnitude at $\alpha = 40°$ by increasing R_∞ from 1.15×10^6/ft to 3×10^6/ft. This data set emphasizes the necessity of obtaining sufficient Reynolds number range at subsonic test conditions to adequately define the effect of crossflows (separation, reattachment, vortices, etc.) on the aerodynamics of this class of candidate VTVL vehicles at high angles of attack. The influence of these effects on full scale vehicles remain to be proved by 6-degree of freedom simulation combining aerodynamics with full scale weights and inertias.

Hypersonic Aerodynamics

The effect of bottom control flap deflections on longitudinal body axis results for the 0.1 r_n/h_b nose configuration at $M_\infty = 10$ and $R_\infty \approx 2 \times 10^6$/ft for a center of gravity at 70% of the virtual length are presented in fig. 8. Increasing deflection produced increasing forces and moments as would be expected. The larger deflections (30° and 40°) created inflections in the force and moment curves indicating a different level of effectiveness due to some local occurance. For example, at $\alpha = -2°$, deflections of 30° and 40° produced increases in slope of the C_N vs. α and C_A vs. α curves and a decrease the slope of the C_m vs α curve. These effects were more pronounced on pitching moment [fig. 8(c)]. The configuration was unstable about the 70% c.g. location with deflected controls rotating the C_m vs. α curve rather than translating it. A 10° deflection produced a stabilizing influence but C_m remained positive and increased with increasing α. Near neutral stability was produced for $\delta_b = 20°$ at negative C_m indicating control deflections between 10° and 20° could produce trim at $M_\infty = 10$ for angles of attack from 0° to over 20°. Deflections of 30° and 40° produced large stabilizing moments, and similar to C_N and C_A, discontinuities in the curves at $\alpha = -2°$. A gradual reduction in this negative C_m production occurred at positive angles of attack.

Figure 9 shows surface streamlines patterns via the oil flow technique. These data augment a $M_\infty = 10$ heating study for this same vehicle and define surface flow characteristics capable of producing the variations in forces and moments shown in fig. 8. The side and top flaps are deflected 10° for the patterns illustrated in fig. 9 compared to zero deflection for the forces and moments presented in fig. 8. However, the bottom (or windward) flap is deflected 20° [figs. 9 (a) and 9(b)] and 30° [figs. 9(c) and 9(d)]. At $\alpha = 0°$ the patterns on the flat area ahead of the hingeline and flap imply some separation occurs ahead of the hinge line with reattachment occurring on the flap. At $\alpha = 15°$ [fig. 9(b)] the cross flow is clearly defined with separation occurring on the flat area in front of the flap hinge line and strong reattachment and recirculation occurring on the flap. At $\alpha = 0°$ deflecting the flap 30° separates the flow over the aft third of the vehicle. In this type of separation, surface pressure is generally higher than in the attached case and this would produce higher forces and nose down moments than in the attached case. Increasing α to 17.5° produces a greatly reduced separated area tending to produce forces and moments closer to what would be expected for attached flow. The line across the rear of the flap is due to body shock ,flap shock interaction that apparently had no significant effect on forces and moments.

The effect of nose bluntness and directional control on directional stability are presented in fig. 10. At all control deflections increasing nose bluntness produced a stabilizing influence. The vehicle with no control deflection was unstable. Deflections greater than 20° were required to produce stability for the 0.1 r_n/h_b nose configuration; $\delta_r = 20°$ was sufficient to produce positive to neutral directional stability for 0.3 r_n/h_b configuration for $\alpha = 0°$ to 20°.

Concluding Remarks

A substantial experimental aerodynamic data base for a candidate vertical takeoff/vertical landing single stage to orbit concept was produced across the subsonic to hypersonic speed regime by testing a single model in a family of wind tunnels. Summary results for this spherically blunted 8° half angle conical forebody, cylindrical afterbody configuration showed increasing Mach number generally reduced lift curve slope and minimum drag. The effect of increasing Mach number on longitudinal stability depended strongly on nose bluntness. Increasing nose bluntness generally reduced lift curve slope, increased minimum drag and produced a stabilizing influence on moments. Adding fin like landing gear housings increased lift curve slope and minimum drag and improved stability.

Possible "anomalies" exist at each end of the operational speed range. At subsonic speeds large side loads, probably due to unsymmetrical lee side vortex sheading at, $\alpha > 20°$ were observed. Increased Reynolds number at subsonic conditions had a stabilizing effect on vortex effects reducing side loads significantly. This emphasizes the need to determine

Reynolds number effects on VTVL vehicles that may operate at high angles of attack at subsonic speeds. At $M_\infty = 10$, control deflections above 20° produced large separated regions at low angles of attack that strongly influenced forces and moments.

References

[1]Henry, Beverly Z. and Decker, John P.: Future Earth Orbit Transportation Systems/Technology Implications. Astronaut. & Aeronaut., vol. 14, no. 9, Sept. 1976, pp. 18-28.

[2]Freeman, Delma C., Jr. and Powell, Richard W.: Impact of Far-Aft Center of Gravity for a Single-Stage-To-Orbit Vehicle. Journal of Spacecraft and Rockets, vol. 17, no. 4, July-August 1980, pp. 311-315.

[3]"Access to Space Study-Summary Report, Office of Space Systems Development," NASA Headquarters, January 1994.

[4]Blase, W. Paul: The First Reusable SSTO Spacecraft. Spaceflight, vol. 35, March 1993, pp. 90-94.

[5]Anon: ViGYAN Low Speed Wind Tunnel

[6]McGhee, Robert J.; Beasley, William D.; and Foster, Jean M.: Recent Modifications and Calibration of the Langley Low Turbulence Pressure Tunnel. NASA TP 2328, July 1984.

[7]Jackson, C. M., Jr.; Corlett, W. A.; and Monta, W. J.: Description and Calibration of the Unitary Plan Wind Tunnel. NASA TP 1905, November 1981.

[8]Miller, C. G., III: Langley Hypersonic Aerodynamic/Aerothermodynamic Testing Capabilities-Present and Future. AIAA Paper 90-1376, 1990.

[9]Braslow, A. L. and Know, E. C.: Simplified Method for Determination of Critical Height of Distributed Roughness Particles for Boundary-Layer Transition at Mach Numbers from 0 to 5. NACA TN 4363, 1958.

[10]Hall, R. M.: Forebody and Missile Side Forces and the Time Analogy. AIAA Paper 87-0327, presented at the AIAA 25th Aerospace Sciences Meeting, January 12-15, 1987, Reno, Nevada.

[11]Hall, Robert M.: Influence of Reynolds Number on Forebody Side Forces for 3.5 Diameter Tangent-Ogive Bodies. AIAA Paper 87-2274, presented at the AIAA 5th Applied Aerodynamics Conference, Monterey, CA, August 17-19, 1987.

Table 1. - VTVL Facility Test Matrix

Facility	Test section size	Pt, psi	Tt,°R	Mach no.	Reynolds no, millions	α	β
ViGYAN	3 ft. x 4 ft.	14.7	520	0.15	1.15 / ft.	-5° to 60°	0°, 5°
LTPT	7.5 ft. x 3 ft.	14.7 to 50	525	0.1 to 0.25	1.6 to 4.9	10° to 45°	0°, 5°
UPWT #1	4.5 ft sq.	7.5 to 11	585	1.6, 2.5	2.0 / ft	-5° to 20°	0°, 5°
UPWT #2	4.5 ft sq.	11 to 32	585 to 610	2.5 to 4.5	2.0 / ft	-5° to 20°	0°, 5°
20 in. M=6	20 in. sq.	100, 225	800, 850	6	2.0 / ft, 4.0 / ft	-5° to 20°	0°, 5°
31 in. M=10	31 in. sq.	350 to 1460	1800	10	0.5 / ft to 2.0 / ft	-5° to 20°	0°, 5°

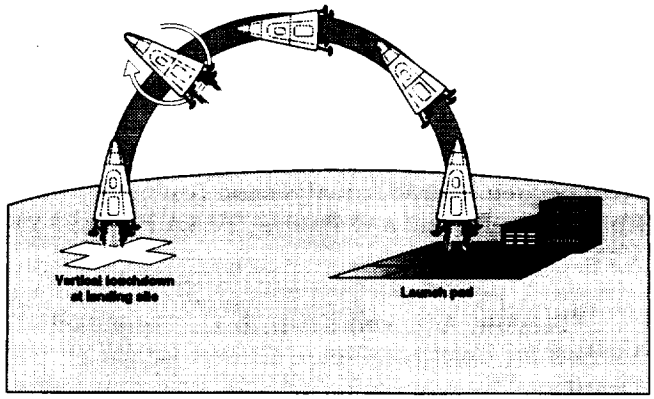

Figure 1. - Delta Clipper flight trajectory

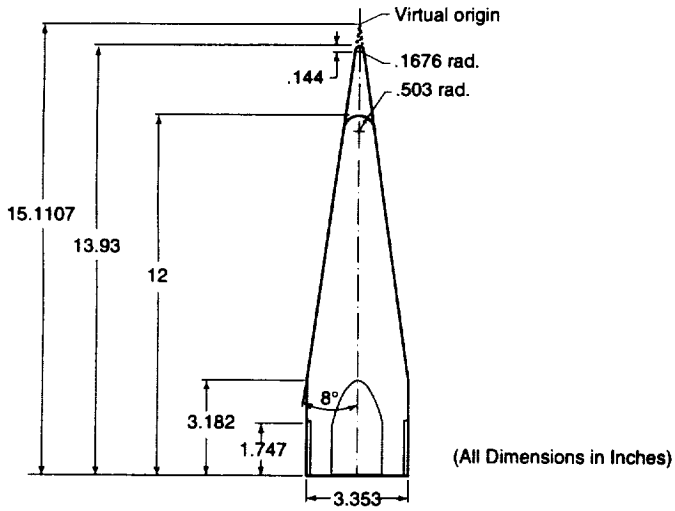

(a.) Basic geometry

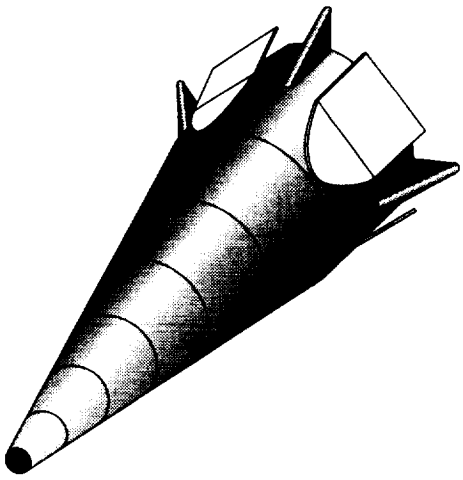

(b) Sketch of complete configuration

Figure 2.- Model geometry

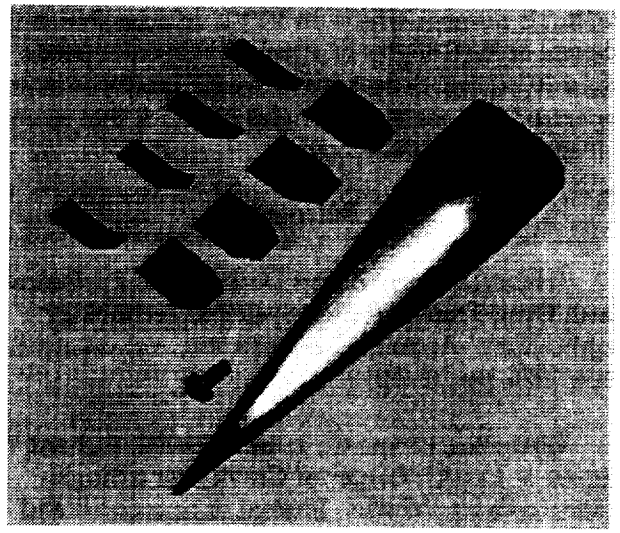

Figure 3. Model photograph

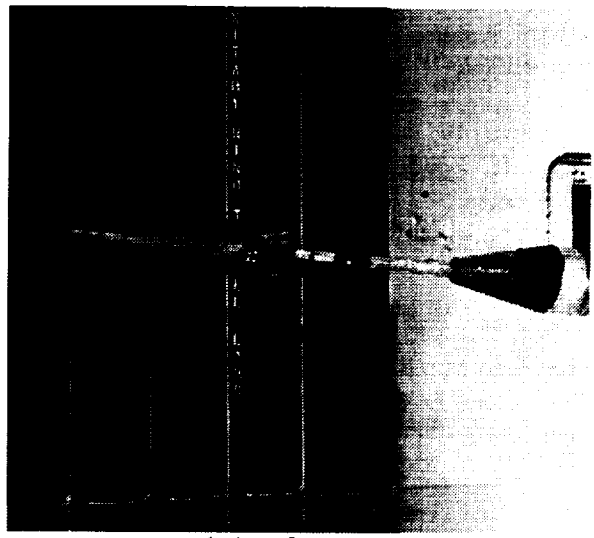

(a.) $r_n/h_b = 0.1$

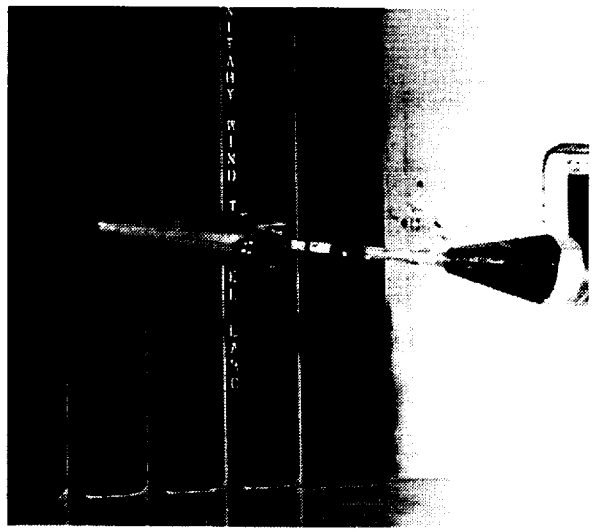

(b.) $r_n/h_b = 0.3$

Figure 4.- Model installation in UPWT #1

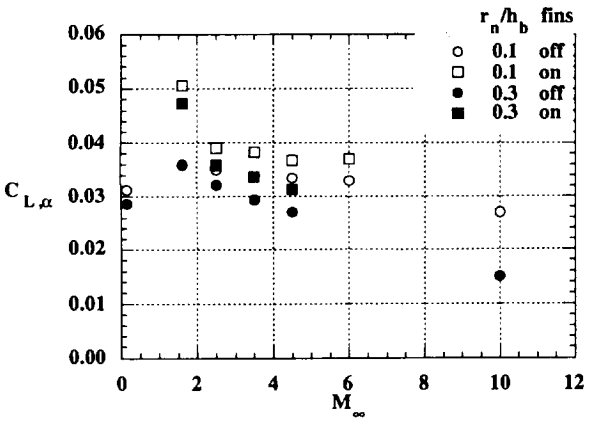

(a.) $C_{L,\alpha}$ vs M_∞

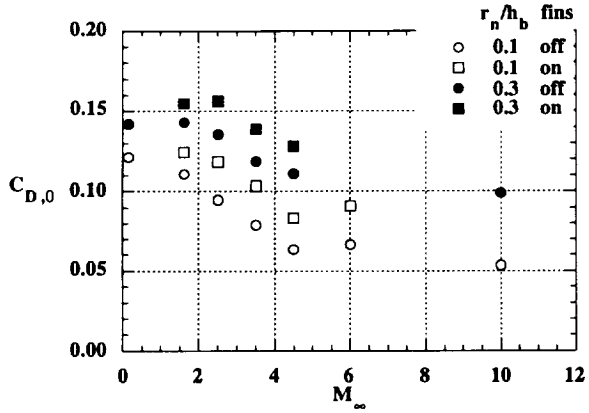

(b.) $C_{D,o}$ vs M_∞

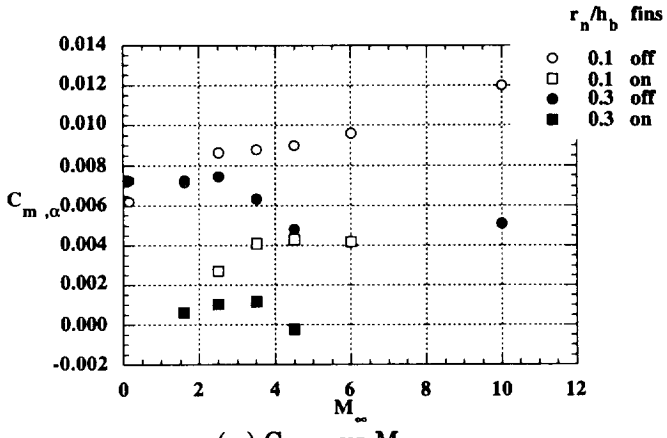

(c.) $C_{m,\alpha}$ vs M_∞

Figure 5 - Effect of Mach no., landing gear covers, and nose bluntness on VTVL aerodynamic characteristics, R_∞ = 2 x 10^6/ft.

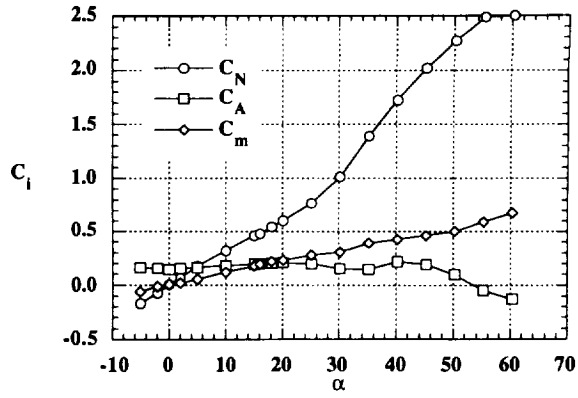

(a.) Longitudinal

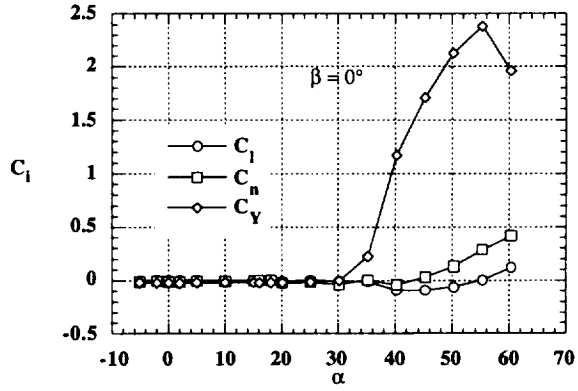

(b.) Lateral/directional

Figure 6. - Subsonic body axis data on the VTVL vehicle, r_n/h_b = 0.3, fins off

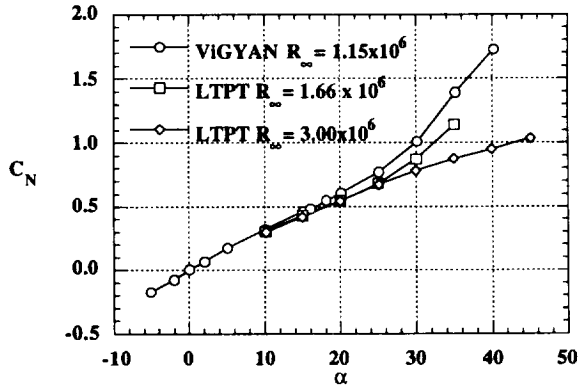

(a.) C_N vs α

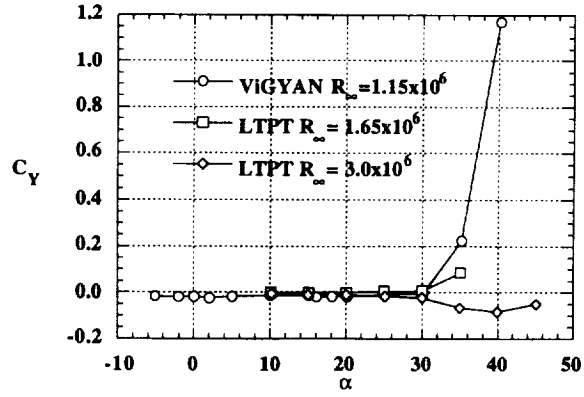

(b.) C_Y vs a

Figure 7. - Effect of Reynolds number at subsonic conditions, r_n/h_b =0.3, fins off.

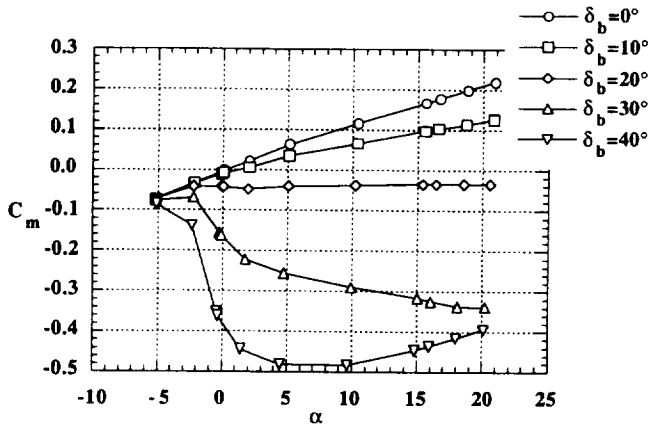

(c.) C_m vs α

Figure 8. - Hypersonic body axis data on the VTVL vehicle, r_n/h_b= 0.1, M_∞ = 10, R_∞ = 2 x 10^6/ft, $x_{c.g.}$ = $0.7L_V$, fins off.

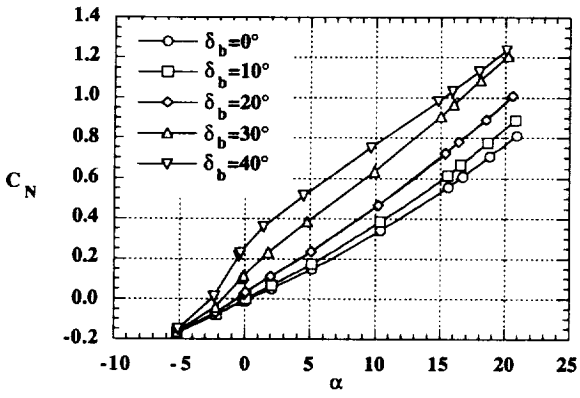

(a.) C_N vs α

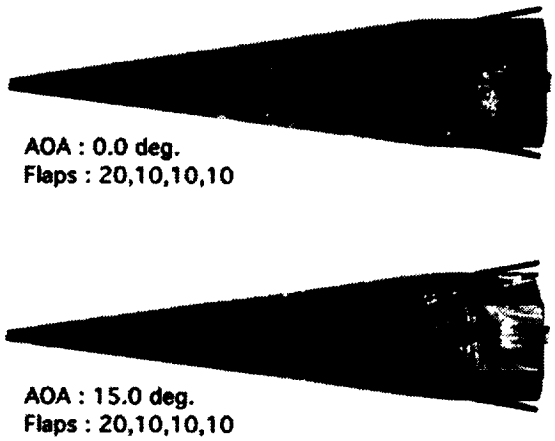

(a.) δ_b = 20°

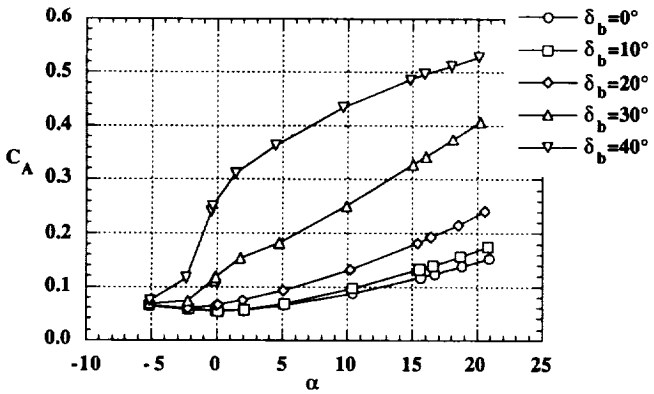

(b.) C_A vs α

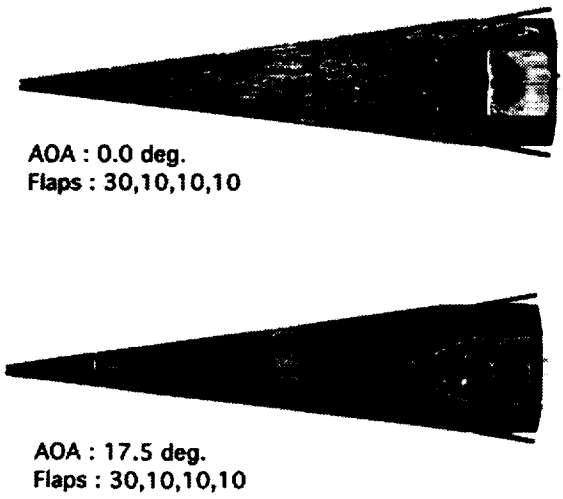

(b.) $\delta_b = 30°$

Figure 9. - Oilflow visualization on the VTVL vehicle at $M_\infty = 10$, $R_\infty = 2 \times 10^6$

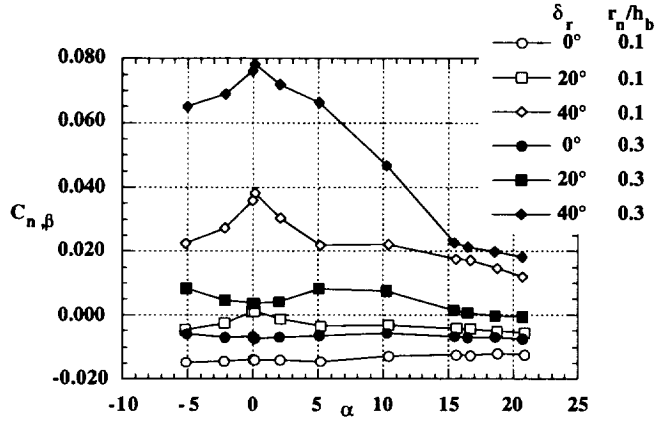

Figure 10. - Effect of nose bluntness and right control flap on directional stability at $M_\infty = 10$, $R_\infty = 2 \times 10^6$